THE JOURNAL OF PHYSICAL CHEMISTRY A

pubs.acs.org/JPCA Article

A Proposed Method to Obtain Surface Specificity with Pump−Probe and 2D Spectroscopies

Megan K. Petti, Joshua S. Ostrander, Erin R. Birdsall, Miriam Bohlmann Kunz, Zachary T. Armstrong, Ariel M. Alperstein, and Martin T. Zanni*

Cite This: J. Phys. Chem. A 2020, 124, 3471−3483 Read Online

ACCESS | Metrics & More | Article Recommendations | Supporting Information

ABSTRACT: Surfaces and interfaces are ubiquitous in nature. From cell membranes, to photovoltaic thin films, surfaces have important function in both biological and materials systems. Spectroscopic techniques have been developed to probe systems like these, such as sum frequency generation (SFG) spectroscopies. The advantage of SFG spectroscopy, a second-order spectroscopy, is that it can distinguish between signals produced from molecules in the bulk versus on the surface. We propose a polarization scheme for third-order spectroscopy experiments, such as pump−probe and 2D spectroscopy, to select for surface signals and not bulk signals. This proposed polarization condition uses one pulse perpendicular compared to the other three to isolate cross-peaks arising from molecules with polar and uniaxial (i.e., biaxial) order at a surface, while removing the signal from bulk isotropic molecules. In this work, we focus on two of these cases: XXXY and YYYX, which differ by the sign of the cross-peak they create. We compare this technique to SFG spectroscopy and vibrational circular dichroism to provide insight to the behavior of the cross-peak signal. We propose that these singularly cross-polarized schemes provide odd-ordered spectroscopies the *surface-specificity* typically associated with even-ordered techniques.

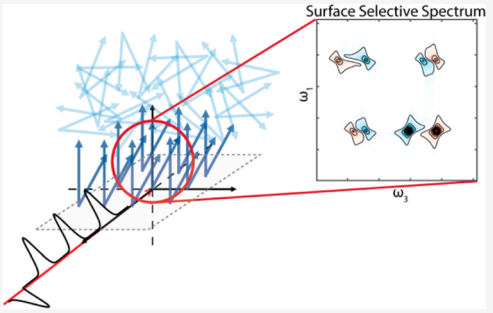

INTRODUCTION

Molecules on a surfaces or at interfaces are known to align in some amount of order, which is important for many branches of chemistry. Ordering can occur in one-direction (uniaxial) or two-directions (biaxial). Examples of these types of ordered systems are depicted in Figure 1B. At the top of the figure are two examples of biaxial systems, an α-helical peptide in a lipid bilayer[1,2] and a small molecule, α-pinene, on a silica surface.[3] Both of these systems have a specified tilt (θ) and twist angle (ψ) relative to the surface, making them biaxial systems. A system that might be expected to be largely uniaxial is water at an air interface (Figure 1B, bottom).[4,5] Here, there is a defined tilt angle (θ), but the molecules might sample all twist angles (ψ). In this work, we focus on surface systems with biaxial order or nonuniform uniaxial order. Other systems that contain biaxial order include membrane proteins within lipid bilayers,[6,7] self-assembled monolayers,[8−10] polymer films,[11−14] catalytic molecules tethered to a surface,[15,16] and some liquid crystals.[17,18] These systems have reduced symmetry at a macroscopic level due to the molecular alignment that can alter chemical and material properties of the system.

In general, molecules at surfaces and interfaces are difficult to study because they are few in number and are usually overwhelmed by signal from the bulk. However, there are linear and nonlinear spectroscopies well suited to the task.[19,20] These nonlinear techniques can be divided into two categories: *surface-sensitive* and *surface-specific*. In general, any technique can be *surface-sensitive*, as it only requires the technique to have adequate sensitivity to measure the small number of molecules present in a surface system, such as a monolayer of chemisorbed molecules.[16,21−23] Some examples of *surface-sensitive* 2D spectroscopic techniques in the infrared is the work of Fayer and Hamm. Fayer has shown that 2D IR spectroscopy has the sensitivity to measure a single monolayer when the local oscillator intensity is reduced at an interface.[9,24,25] Hamm has taken a different approach and used an attenuated total reflection (ATR) geometry in combination with localized surface plasmons of metallic nanoparticle-coated surfaces to provide enhancement of the signal of molecules near the surface.[26−29]

Surface-specific techniques, on the other hand, are only able to detect signals that are produced by molecules at a surface or interface and not the signals from molecules present in the bulk, such as at an interface of two bulk materials.[4,30−34] Normally, the technical distinction between *surface-sensitive* and *surface-specific* nonlinear techniques is the order of the susceptibility measured. For example, sum frequency generation (SFG) spectroscopy is

Received: December 20, 2019
Revised: March 27, 2020
Published: April 7, 2020

https://dx.doi.org/10.1021/acs.jpca.9b11791
J. Phys. Chem. A 2020, 124, 3471−3483

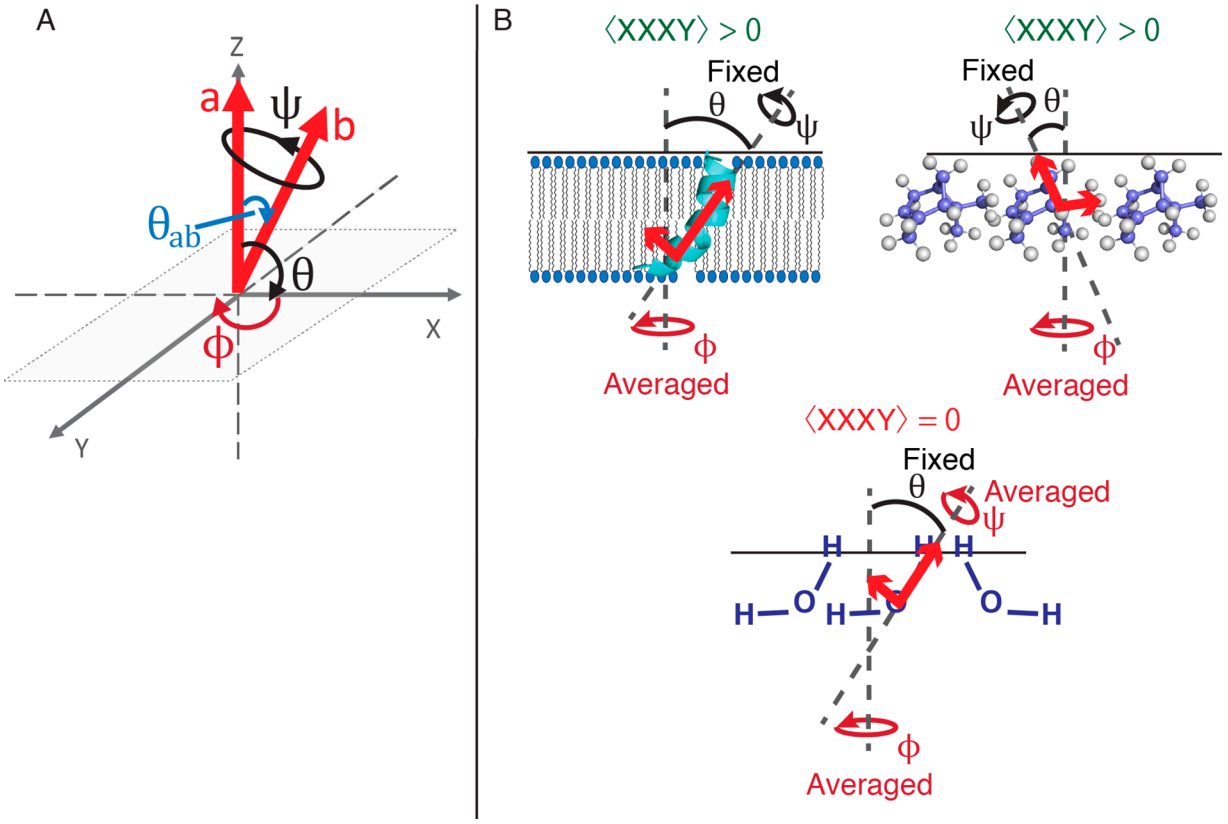

Figure 1. (A) Schematic of the orientation of two coupled oscillators, a and b, depicted as red arrows in *XYZ* space. ϕ is the *XY* plane, θ is in the *ZX* plane, and ψ is twist angle of the oscillators. *Z* is the direction light is propagating. (B) Examples of surface systems that have biaxial symmetry (top) and an example that does not have biaxial symmetry (bottom).

an even-ordered spectroscopy that measures the second-order susceptibility and is inherently sensitive to surfaces.[35,36] In general, even-ordered susceptibilities of a centrosymmetric media, like a bulk solution, average to zero in the dipole approximation.[37] However, if the symmetry of the system is broken, like at an interface, then the even-ordered susceptibilities become significant. Because of this dependence on the symmetry of the system, even-ordered spectroscopies only measure signals from interfacial molecules, without any interference of bulk signals, making these techniques *surface-specific*.[38] Typically, odd-ordered spectroscopies cannot make this same type of distinction as the susceptibilities from both the bulk system and the surface system will be relevant regardless of the centrosymmetry of the system.

At the microscopic level, a reduction of symmetry can occur when an individual component of a system has a specified direction, such as when a molecule has a chiral center. Being able to distinguish between enantiomers requires measuring signatures that are intrinsic to a specific chirality. Circular dichroism is able to accomplish this distinction. Vibrational circular dichroism (VCD) measures the optical activity related to how chiral molecules interact with left versus right circularly polarized infrared light to produce a differential absorption spectra (left-circularly polarized minus right-circularly polarized light).[39−41] Thus, one enantiomer (R-) will produce absorption features with an opposite sign of that of the complementary enantiomer (S-). A racemic mixture of molecules will not produce a VCD signal, as the absorption of the two enantiomers will cancel out. Because of this dependence on the molecular structure, VCD has been used to obtain structural information on chemical and biological systems.

In the work presented here, we propose that *surface-specific* information can be obtained from an odd-order (in this case, third-order) experiment for a biaxial surface, meaning that the system has both uniaxial order over the twist (ψ) angle and polar order over the tilt angle (θ). The key is to set one of the pulses perpendicular to the other three in the four-wave mixing process. The same trick can be applied to other third-order techniques, like pump−probe spectroscopy. This polarization condition selects for third-order cross-peaks pathways from molecules at the surface, while the third-order pathways from molecules in the bulk are zero, effectively extending odd-ordered spectroscopies into a *surface-specific* domain. This work is similar to the chirality-induced 2D, a two-dimensional analogue of VCD, spectroscopy proposed by Mukamel and colleagues employing the same polarization scheme.[42,43] The difference is that our work is completely dipole allowed and does not require the molecule to be inherently chiral. The only requirements are (1) that there is macroscopic uniaxial and polar order at the surface and (2) that the molecule or molecules of interest have coupled and nonparallel transition dipoles. A similar approach has been proposed to measure surface-specific signals in nonlinear Raman and linear fluorescence spectroscopic measurements.[44,45] In this manuscript, we provide the mathematical background and simulated 2D spectra to describe this singularly cross-polarized technique. We also compare our work with SFG spectroscopy and VCD to elaborate on the similarities and differences with our proposed technique.

https://dx.doi.org/10.1021/acs.jpca.9b11791
J. Phys. Chem. A 2020, 124, 3471−3483

COMPUTATIONAL DETAILS

Two-dimensional third-order spectroscopies can be thought of as frequency resolved pump−probe techniques that disperse the frequencies of the pump along one axis and the probe along the other.[46−49] This creates a two-dimensional energy correlation map that provides information about the orientation and energy transfer of these states. For example, consider a simple small molecule that has two coupled states that absorb at different frequencies. This system results in three major characteristics of the spectrum: diagonal peaks, cross-peaks, and the line shape of these peaks. In this work, we focus on the first two characteristics. The diagonal peaks arise from one state, while the cross-peaks are observed when two states are coupled together. This coupling can be either electronic or mechanical in nature.[49−52]

We are interested in the third-order signals that create these 2D spectrum of both bulk and surface systems. The main difference between these two cases is the macroscopic orientation of the systems, that is, the orientation of an ensemble of molecules. For the bulk system, we consider two coupled oscillators that are dispersed in an isotropic ensemble. For the surface system, we consider two coupled oscillators that are aligned normal to the surface at a specific angle (θ) and have a specified twist angle (ψ) (Figure 1A).

The orientation of each of these systems is mapped onto the third-order signal and can be described generally by a four-point correlation function as follows:[46−48,53]

$$S \propto \langle (\vec{\mu}_\delta \cdot \vec{E}_d)(\vec{\mu}_\gamma \cdot \vec{E}_c)(\vec{\mu}_\beta \cdot \vec{E}_b)(\vec{\mu}_\alpha \cdot \vec{E}_a) \rangle \quad (1)$$

In eq 1, S is the third-order signal that is proportional to the expectation value (represented by the brackets $\langle ... \rangle$) of the dipole operator for one particular Feynman pathway. The light-matter interactions for one such pathway is described by the dot product between four arbitrary transition dipole vectors ($\vec{\mu}_\delta$, $\vec{\mu}_\gamma$, $\vec{\mu}_\beta$, $\vec{\mu}_\alpha$) and electric field vectors ($\vec{E}_d$, $\vec{E}_c$, $\vec{E}_b$, $\vec{E}_a$). This function holds under the semi-impulsive limit and the dipole approximation. This equation can further be separated into the magnitude and the direction of these vectors. By ignoring the magnitude of these vectors, the orientational four-point correlation function is described by eq 2 where we now represent these unit vectors with a hat ($\hat{}$).

$$S \propto \langle (\hat{\mu}_\delta \cdot \hat{E}_d)(\hat{\mu}_\gamma \cdot \hat{E}_c)(\hat{\mu}_\beta \cdot \hat{E}_b)(\hat{\mu}_\alpha \cdot \hat{E}_a) \rangle \quad (2)$$

Equation 2 describes four arbitrary transition dipole directions interacting with four arbitrarily polarized pulses. With this equation, we can calculate the third-order signal in the X, Y, and Z directions by evaluating eq 2. We can do this for the many Feynman pathways that describe the possible light-matter interactions for both bulk and surface systems. We choose to only evaluate the four-point correlation function for eight Feynman pathways (*iiii, jjjj, iijj, ijij, ijji, jjii, jiji, jiij*) that describe 2D spectra. In general, Feynman pathways describe the time ordering of interactions between an oscillator (i or j in this case) with an electric field. A double-sided Feynman diagram, as in Figure 2, allows for visualization of how the dipole operator operates. Arrows pointing to the left operate on the bra side, while arrows pointing to the right operate on the ket side. Figure 2 depicts the rephasing and nonrephasing pathways that contribute to the diagonal peaks and cross-peaks in 2D spectra.

To evaluate eq 2, four steps are required. First, the defined dipoles (a and b in Figure 1A), are rotated into the lab frame.

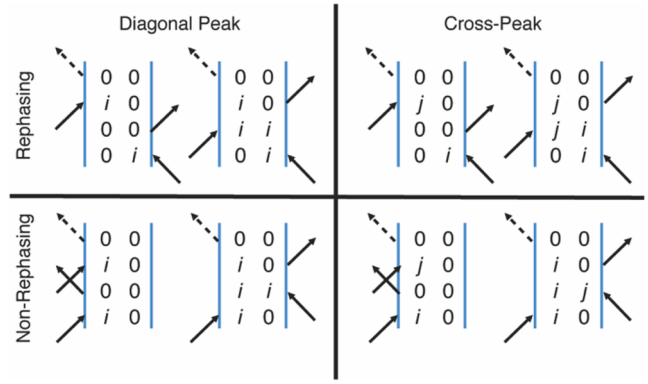

Figure 2. Double-sided Feynman diagrams for arbitrary oscillators i and j for both rephasing and nonrephasing pathways that describe the diagonal and cross-peaks in third-order spectroscopy. The diagonal peaks are shown as interactions only with i and can be represented as *iiii*. The cross-peaks have interactions with both i and j and can be represented as *iijj*, *ijij*, and *ijji*. Note, *ijji* is a nonrephasing pathway, *ijij* is a rephasing pathway, and *iijj* is both.

Then, the third-order susceptibility ($\chi^{(3)}$) is calculated by considering the projection of the lab frame dipoles in three-dimensional space. Next, the third-order polarization ($P^{(3)}$) is calculated by convoluting the calculated susceptibility with polarized electric fields. Lastly, the projection of the third-order polarization in the direction of detection is calculated.[44,48,54]

For the first step in this calculation, we begin by rotating the defined dipoles into the lab frame. To do so, one may use spherical harmonics[55] or a tensor method.[53] We have chosen to use Euler angles to calculate the dependence of the signal on orientation.[54] With this method we first take our two oscillators defined in the molecular frame and rotate them into the lab frame via a Euler rotation matrix. The projection of these lab frame dipoles is then calculated in the X, Y, and Z directions.

Next, the third-order susceptibility is calculated by considering the macroscopic orientation of the system of interest. For the bulk system, the molecules are isotropic; therefore to obtain a macroscopic orientation of the sample, all possible configurations in three-dimensional space must be considered. Thus, the third-order susceptibility is integrated over all space that is defined in spherical coordinates by the three angles: ϕ, θ, and ψ. These angles are evaluated from 0 to 2π, 0 to π, and 0 to 2π, respectively. For the surface system, the surface limits the possible orientations of the molecule, introducing anisotropy and reducing the symmetry of the system. Figure 1A defines the surface system where there are two coupled oscillators, a and b, in the XZ plane (the surface is shown in the XY plane). The angle θ_{ab} separates the two dipoles. In the cases discussed, θ_{ab} is set to 30°. Other values for θ_{ab} have also been evaluated (results shown in Figures S1−S4). In the case where molecules at the surface are highly ordered, the tilt angle (θ), and the twist angle (ψ) are set, creating a system with polar and uniaxial order. In other words, the system is biaxial, leading to ensemble differences only in the ϕ dimension. Thus, for the surface system, the evaluation of the third-order susceptibility need only be evaluated over ϕ. In general, systems that satisfy this type of symmetry are self-assembled monolayers, thin-films, lipid bilayers, and surface oriented membrane proteins monolayers.[15,56,57]

We then calculate the third-order macroscopic polarization by taking the evaluated susceptibilities and accounting for the polarization of each pulse. The resulting macroscopic polarization is summed over all possible combinations in the X, Y, and

https://dx.doi.org/10.1021/acs.jpca.9b11791
J. Phys. Chem. A 2020, 124, 3471−3483

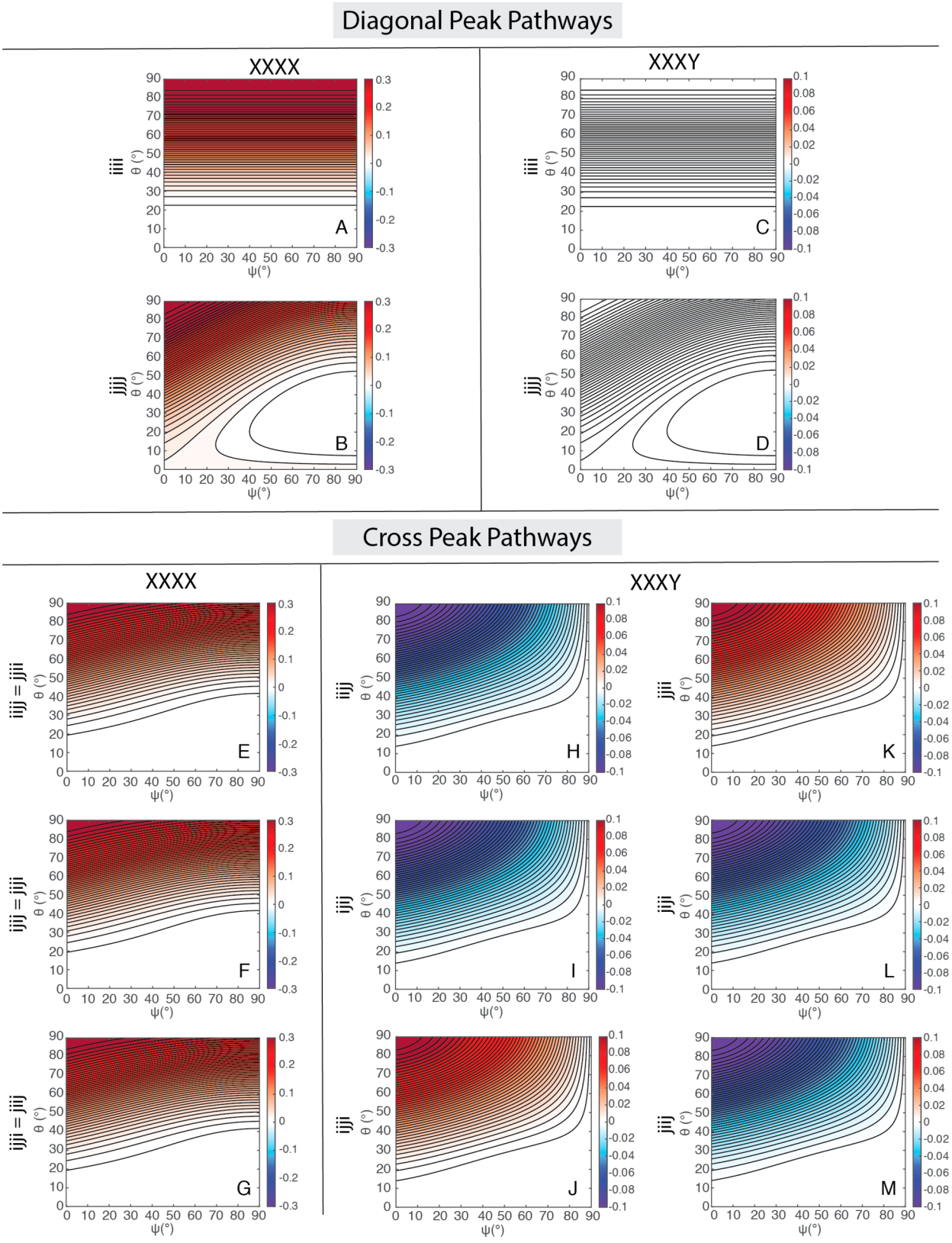

Figure 3. Orientational four-point correlation function values for the pathways *iiii*, *jjjj*, *iijj*, *ijij*, *ijji*, *jjii*, *jiji*, and *jiij* as a function of θ and ψ for the surface system using two different polarization conditions: XXXX and XXXY.

Z directions. We then determine the detected signal by calculating the projection of the signal in all possible directions of detection. We consider two cases for detecting the signal. In the first case, the detected signal is parallel to the incident light, while in the second case the detected signal is perpendicular to the incident light. We distinguish between these polarization conditions by referring to them as either XXXX (parallel detection) or XXXY (perpendicular detection). We note that by

https://dx.doi.org/10.1021/acs.jpca.9b11791
J. Phys. Chem. A 2020, 124, 3471−3483

convention, for four-wave mixing experiments, the polarization notation above refers to the polarization of light used where the fourth interaction is from a local oscillator. In our calculations, we refer to the fourth interaction as the direction of the detected signal, although the use of an external local oscillator would result in the same conclusions. Figure 1A depicts the X and Y directions with the Z direction normal to the surface. The final projections of the third-order macroscopic polarization correspond to the orientational four-point correlation function described by eq 2.

Overall, we evaluate the detected signal for the Feynman pathways associated with third-order spectroscopies for both bulk and surface systems under two polarization conditions; XXXX and XXXY. We then use those results to map how these pathway responses influence the diagonal and cross-peak signals in a 2D spectrum. Additional details of the procedure and simulations are given in the Supporting Information.

RESULTS AND DISCUSSION

In the following, we divide our Results and Discussion into four sections (orientational four-point correlation functions, diagonal and cross-peak intensities, simulated 2D spectra, and comparison to SFG spectroscopy and VCD) to investigate the polarization scheme XXXY from the bottom up. In other words, we begin by evaluating the four-point correlation functions for XXXY and use that information to simulate 2D spectra. This method provides insight into how the XXXY polarization scheme can be used to detect signals from surface systems and not the bulk.

Orientational Four-Point Correlation Functions. The orientational four-point correlation function solutions for isotropic systems have previously been published and are rewritten here in eqs 3 and 4.[48,53] There is no variation in the detected signal as a function of twist (ψ) and tilt (θ) angles (Figure S6).

$$\begin{aligned}&\langle(\hat{\mu}_i\cdot\hat{E}_X)(\hat{\mu}_i\cdot\hat{E}_X)(\hat{\mu}_i\cdot\hat{E}_X)(\hat{\mu}_i\cdot\hat{E}_X)\rangle\\&=\frac{1}{8\pi^2}\int_0^{2\pi}\mathrm{d}\psi\int_0^{\pi}\mathrm{d}\theta\int_0^{2\pi}d\phi\,\sin\theta(\sin\phi\,\sin\theta)^4\\&=\frac{1}{5}\end{aligned}\tag{3}$$

$$\begin{aligned}&\langle(\hat{\mu}_i\cdot\hat{E}_X)(\hat{\mu}_i\cdot\hat{E}_X)(\hat{\mu}_j\cdot\hat{E}_X)(\hat{\mu}_j\cdot\hat{E}_X)\rangle\\&=\frac{1}{8\pi^2}\int_0^{2\pi}\mathrm{d}\psi\int_0^{\pi}\mathrm{d}\theta\int_0^{2\pi}\mathrm{d}\phi\,\sin\theta(\sin\phi\,\sin\theta)^2\\&\quad(\sin\theta_{ab}(-\sin\psi\,\cos\theta\,\sin\phi+\cos\phi\,\cos\psi)\\&\quad+\sin\theta\,\sin\phi\,\cos\theta_{ab})^2\\&=\frac{1}{15}(2(\cos\theta_{ab})^2+1)\end{aligned}\tag{4}$$

For the XXXX polarization conditions for the bulk isotropic system, the constant value is $^1/_5$ for pathways that only interact with one oscillator (*iiii* and *jjjj*). For the other six pathways that involve interactions with both oscillators, the constant value is equivalent for all pathways (*iijj* = *jjii* = *ijij* = *jiji* = *ijji* = *jiij*) and depends on the angle between the two oscillators (θ_{ab}). For the XXXY case, the signal of the bulk system for all pathways goes to zero (Figure S6), because the functions are odd (eqs S17−S19).

Evaluation of the orientational four-point correlation function for the surface system leads to different functions. Because of the order imposed by the surface, the system is azimuthally isotropic, and the resulting third-order susceptibility is integrated over ϕ. This leads to an orientational dependence on the detected signal for the surface system as a function of θ and ψ for all the pathways considered for both XXXX and XXXY (Figure 3). We plot the signal of eight Feynman pathways for the XXXX and XXXY polarization schemes for the surface system as a function of $\theta = 0°-90°$ and $\psi = 0°-90°$. All possible values of θ and ψ have been investigated and can be found in Figure S5. The difference between the two polarization conditions for the surface system is readily apparent. For XXXX, all eight pathways have positive values that depend on the θ and ψ values and the six cross-peak pathways are equivalent (Figure 3E−G). In XXXY, the *iiii* and *jjjj* pathways are zero, while the remaining six cross-peak pathways provide a response as a function of θ and ψ. In other words, the XXXY four-point correlation functions are even-order functions over ϕ for the cross-peak pathways. Thus, these functions are not zero when integrating between 0 and 2π. Moreover, the cross-peak pathways are not equivalent in the XXXY case. For the XXXY polarization configuration, *iijj* = −*jjii*, *ijij* = *jiji*, and *ijji* = −*jiij*. Also, for the *iijj*, *ijij*, *jiji*, and *jiij* pathways, the response has a flipped sign (is now negative) when compared to the XXXX polarization condition. These differences in the pathway response have implications for the sign of the signals observed in an XXXY configuration.

We note that setting any one of the pulses in the four-wave mixing process perpendicular to the other three pulses should produce the same results as XXXY. For the surface system, this means that the diagonal peak pathways are zero, while the cross-peak pathways are not, while for the bulk system, all pathways are zero. There are eight possible polarization schemes (XXXY, XXYX, XYXX, YXXX, YYYX, YYXY, YXYY, and XYYY) that are all able to detect surface signals. However, while the schemes are equivalent for the *iiii* and *jjjj* pathways, the schemes are not completely equivalent for the off-diagonal cross-peak total functions. For the surface system, we outline these differences by calculating the total four-point correlation function for an off-diagonal cross-peak (the *i*-*j* cross-peak) for two of these eight possible schemes: XXXY and XXYX.

The pathways that make up the *i*−*j* off-diagonal cross-peak are the rephasing *ijij*, rephasing *iijj*, and nonrephasing *iijj* pathways. In the argument that follows we assume that all pathways contribute equally. If the contributions of the pathways were unequal, the intensity of the peaks in the spectra would be modulated. In the XXXY polarization configuration, the *ijij* and *iijj* pathways are equivalent. For these pathways, there are two interactions with oscillator *i* in the X direction, one interaction with *j* in the X direction, and one interaction with *j* in the Y direction. Equation 5 evaluates the orientational four-point correlation function for the surface with a XXXY polarization scheme for both the *ijij* and *iijj* pathways.

$$\begin{aligned}&\langle(\hat{\mu}_i\cdot\hat{E}_X)(\hat{\mu}_j\cdot\hat{E}_X)(\hat{\mu}_i\cdot\hat{E}_X)(\hat{\mu}_j\cdot\hat{E}_Y)\rangle\\&=\langle(\hat{\mu}_i\cdot\hat{E}_X)(\hat{\mu}_i\cdot\hat{E}_X)(\hat{\mu}_j\cdot\hat{E}_X)(\hat{\mu}_j\cdot\hat{E}_Y)\rangle\\&=\frac{1}{2\pi}\int_0^{2\pi}\mathrm{d}\phi(\sin\phi\,\sin\theta)^2(\sin\theta_{ab}(-\sin\psi\,\cos\theta\,\sin\phi\\&\quad+\cos\phi\,\cos\psi)+\sin\theta\,\sin\phi\,\cos\theta_{ab})\\&\quad(\sin\theta_{ab}(-\sin\psi\,\cos\theta\,\cos\phi-\sin\phi\,\cos\psi)+\sin\theta\,\sin\phi\,\cos\theta_{ab})\\&=-\frac{\cos\psi\,\sin\theta_{ab}(\sin\theta)^2}{4}(\cos\theta_{ab}\,\sin\theta-\cos\theta\,\sin\psi\,\sin\theta_{ab})\end{aligned}\tag{5}$$

https://dx.doi.org/10.1021/acs.jpca.9b11791
J. Phys. Chem. A 2020, 124, 3471−3483

On the other hand, when we consider the *ijij* and *iijj* pathways in XXYX, the pathways are not equivalent. In the case of *iijj*, there are two interactions with oscillator *i* in the *X* direction, one interaction with oscillator *j* in the *X* direction, and one interaction with oscillator *j* in the *Y* direction. For *ijij*, there are instead two interactions with oscillator *j* in the *X* direction, one interaction with oscillator *i* in the *X* direction, and one interaction with oscillator *i* in the *Y* direction. These lead to two different four-point correlation functions for the *ijij* and *iijj* pathways in the XXYX polarization scheme. These are evaluated in eqs 6 and 7.

$$\begin{aligned}&\langle(\hat{\mu}_i\cdot\hat{E}_X)(\hat{\mu}_j\cdot\hat{E}_X)(\hat{\mu}_i\cdot\hat{E}_Y)(\hat{\mu}_j\cdot\hat{E}_X)\rangle\\&=\frac{1}{2\pi}\int_0^{2\pi}\mathrm{d}\phi\,\sin\phi\,\sin\theta(\sin\theta_{ab}(-\sin\psi\,\cos\theta\,\cos\phi-\sin\phi\,\cos\psi)\\&\quad+\sin\theta\,\sin\phi\,\cos\theta_{ab})^2\cos\phi\,\sin\theta\\&=\frac{\cos\psi\,\sin\theta_{ab}(\sin\theta)^2}{4}(\cos\theta_{ab}\,\sin\theta-\cos\theta\,\sin\psi\,\sin\theta_{ab})\end{aligned}\tag{6}$$

$$\begin{aligned}&\langle(\hat{\mu}_i\cdot\hat{E}_X)(\hat{\mu}_i\cdot\hat{E}_X)(\hat{\mu}_j\cdot\hat{E}_Y)(\hat{\mu}_j\cdot\hat{E}_X)\rangle\\&=\frac{1}{2\pi}\int_0^{2\pi}\mathrm{d}\phi(\sin\phi\,\sin\theta)^2(\sin\theta_{ab}(-\sin\psi\,\cos\theta\,\sin\phi\\&\quad+\cos\phi\,\cos\psi)+\sin\theta\,\sin\phi\,\cos\theta_{ab})\\&\quad(\sin\theta_{ab}(-\sin\psi\,\cos\theta\,\cos\phi-\sin\phi\,\cos\psi)+\sin\theta\,\sin\phi\,\cos\theta_{ab})\\&=-\frac{\cos\psi\,\sin\theta_{ab}(\sin\theta)^2}{4}(\cos\theta_{ab}\,\sin\theta-\cos\theta\,\sin\psi\,\sin\theta_{ab})\end{aligned}\tag{7}$$

These differences in the orientational four-point correlation functions of the *iijj* and *ijij* pathways leads to a different value for the total function that defines the off-diagonal cross-peak that depends on the polarization used. In the case of XXXY, where the rephasing *ijij*, rephasing *iijj*, and nonrephasing *iijj* are equivalent, then the total contribution to the off-diagonal cross-peak will just be three times that of eq 5. This total function is expressed in eq 8. For XXYX, *ijij* and *iijj* have four-point correlation functions that differ in the sign of the function; *iijj* is the negative of *ijij*. To obtain the total, we add the function for *ijij* (eq 6) to twice that of the function for *iijj* (eq 7) (to account for the rephasing and nonrephasing pathways contributions), leading to the result in eq 9 for the total off-diagonal cross-peaks in XXYX:

$$\begin{aligned}&\mathrm{XXXY}_{\text{off-diagonal cross-peak}}\\&=-\frac{3\cos\psi\,\sin\theta_{ab}(\sin\theta)^2}{4}(\cos\theta_{ab}\,\sin\theta\\&\quad-\cos\theta\,\sin\psi\,\sin\theta_{ab})\end{aligned}\tag{8}$$

$$\begin{aligned}&\mathrm{XXYX}_{\text{off-diagonal cross-peak}}\\&=-\frac{\cos\psi\,\sin\theta_{ab}(\sin\theta)^2}{4}(\cos\theta_{ab}\,\sin\theta\\&\quad-\cos\theta\,\sin\psi\,\sin\theta_{ab})\end{aligned}\tag{9}$$

Equation 8 and eq 9 provide the following relationship between the polarization conditions XXXY and XXYX for the surface system:

$$\mathrm{XXXY}_{\text{off-diagonal cross-peak}}=3\mathrm{XXYX}_{\text{off-diagonal cross-peak}}\tag{10}$$

Equation 10 shows that the off-diagonal cross-peak intensity of XXXY will be three times that of the off-diagonal cross-peak intensity in XXYX. We can do this same analysis of the orientational four-point correlations functions for the other six polarization schemes to determine the relationships between them. Table 1 depicts these relationships. The evaluated orientational four-point correlation functions for the remaining six polarization schemes can be found in the Supporting Information (eqs S3−S16). It should be noted that while this argument only considers the *i*−*j* cross-peak, the same conclusions can be made when considering the *j*−*i* cross-peak.

Table 1. Relationships between All Possible Singularly Cross-Polarized Cross-Peak Four-Point Correlation Functions

mostly *X* interactions	mostly *Y* interactions
XXXY = 3XXYX	YYYX = 3YYXY
YXXX = 3 XYXX	XYYY = 3YXYY
overall relationships	
XXXY = −YXXX = −YYYX = XYYY	
XXYX = −XYXX = −YYXY = YXYY	

Diagonal and Cross-Peak Intensities. The differences between the bulk and surface systems pathways shown in Figure S6 and Figure 3 ultimately influence the 2D spectra collected. By considering what pathways contribute to which peaks, we can elucidate how the diagonal and cross-peaks differ between the bulk and surface systems. The *iiii* and *jjjj* pathways correspond to diagonal peaks. The *iijj* and *ijij* pathways correspond to the lower *i*−*j* cross-peak (as oscillator *i* is set to absorb at a lower energy), and the *jjii* and *jiji* pathways correspond to the upper *j*−*i* cross-peak. The nonrephasing *ijji* and the nonrephasing *jiij* pathway contain cross-peaks that appear on the diagonal. We plot the normalized (to the maximum value) diagonal and cross-peak intensity dependence on θ and ψ for both bulk and surface systems in Figure 4. It is assumed that each pathway contributes equally. As before, we consider the XXXX and XXXY polarization conditions. For the bulk, we obtain the expected result. For the XXXX polarization, there is no dependence on θ and ψ angles as the macroscopic orientation is isotropic, leading to a constant value (Figure 4A and Figure 4F). In this case, the constant value is negative and corresponds to the ground state bleach. For the XXXY case, the bulk response goes to zero for both the diagonal and cross-peaks (Figure 4B and Figure 4G), consistent with the values obtained for the bulk pathways (Figure S6). For the surface system, the diagonal and cross-peak responses are different between the two polarization cases. For the XXXX case, the diagonal and cross-peak responses of the surface have a negative response that depends on the θ and ψ values of the system, corresponding to ground state bleach (Figure 4C and Figure 4H). However, this is not true for the XXXY case. Here, the diagonal and cross-peak responses are different signs (Figure 4D,E and Figure 4I,J, boxed in gray). The *i* diagonal peak intensity is solely from the nonrephasing *ijji* pathway that has an on-diagonal cross-peak, and the *j* diagonal peak is from the nonrephasing *jiij* pathway. These have opposite signs relative to each other, just like the pathway responses in Figure 3J and Figure 3M. The other pathways that contribute to the diagonal peaks (*iiii* and *jjjj*) are zero as seen in Figure 3C,D. Thus, the only signals observed from a surface detected in XXXY result from cross-peak pathways. The sign of the upper (*j*−*i*) and lower (*i*−*j*) off-diagonal cross-peaks are also opposite (Figure 4I,J) from each other. Moreover, the fact that the lower off-diagonal cross-peak has the opposite sign between the XXXY and XXXX configurations is a signature of the surface response. This sign change is a direct consequence of the sign of the *iijj*, *ijij*,

https://dx.doi.org/10.1021/acs.jpca.9b11791
J. Phys. Chem. A 2020, 124, 3471−3483

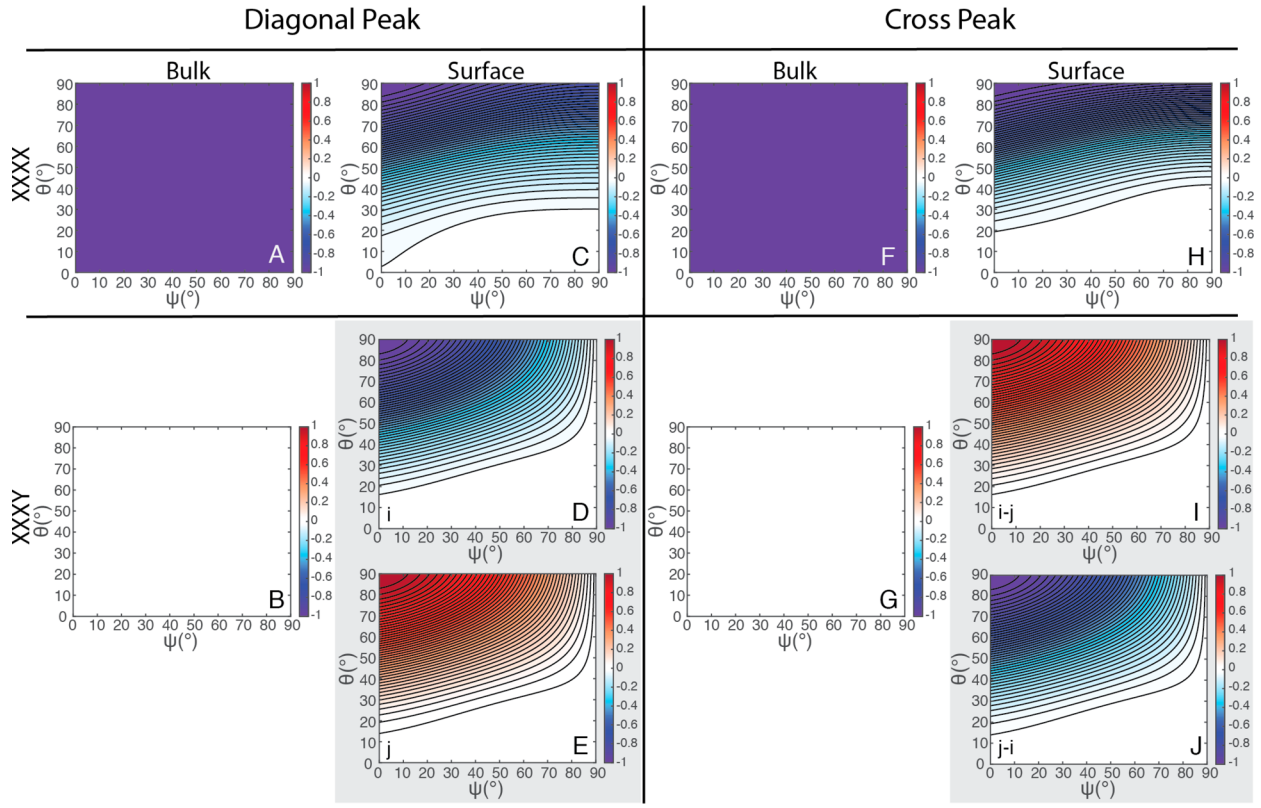

Figure 4. Normalized diagonal and cross peak dependences on θ and ψ angles for both bulk and surface systems for two different polarization conditions: XXXX and XXXY.

jjii, and *jiji* pathways. The sign change provides clear indications for detecting the signal only from molecules at the surface.

Simulated Two-Dimensional Spectra. We further investigate the surface response by simulating representative 2D spectra of two coupled oscillators based on our calculations above. In these simulations, two well-separated arbitrary wavelengths are defined for oscillator *i* and oscillator *j*. *i* and *j* correspond to the lower energy and higher energy transition, respectively. This diagonalized Hamiltonian uses fixed diagonal and off-diagonal anharmonicities by assuming that the oscillators are close to harmonic and thus scale as $\mu_{12}^2 = 2\mu_{01}^2$. The angle between the two dipoles (θ_{ab}) is set to 30° as in the calculations above. Using the original dipoles defined in Figure 1, the coupling term (β) is found between the two oscillators (eq S26). This coupling constant is then used to determine the mixing angle (α) between the two dipoles (eq S29). On the basis of this mixing angle, the two dipoles are redefined (eqs S30 and S31). The magnitude of these new vectors defines the transition dipole strength. This transformation effectively maps the relative orientation and the coupling of the dipoles to the intensity of the transitions. The 2D spectra are simulated by using the orientational response of each pathway calculated in Figure 3 and weighting them by the transition dipole strength. These values are then plugged into the third-order rephasing and nonrephasing response functions. Equations 11 and 12 are representative rephasing ($R_1^{(3)}$) and nonrephasing ($R_4^{(3)}$) response functions for the diagonal peaks of one oscillator, *i*.

$$R_1^{(3)}(t_3, t_2, t_1) \propto -\langle(\hat{\mu}_i\cdot\hat{E}_d)(\hat{\mu}_i\cdot\hat{E}_c)(\hat{\mu}_i\cdot\hat{E}_b)(\hat{\mu}_i\cdot\hat{E}_a)\rangle|\mu_i|^4 \, e^{i\omega_i(t_1-t_3)-(t_1+t_3)/T_2} \quad (11)$$

$$R_4^{(3)}(t_3, t_2, t_1) \propto -\langle(\hat{\mu}_i\cdot\hat{E}_d)(\hat{\mu}_i\cdot\hat{E}_c)(\hat{\mu}_i\cdot\hat{E}_b)(\hat{\mu}_i\cdot\hat{E}_a)\rangle|\mu_i|^4 \, e^{-i\omega_i(t_1+t_3)-(t_1+t_3)/T_2} \quad (12)$$

In eqs 11 and 12, the term in the brackets, $\langle(\hat{\mu}_i\cdot\hat{E}_d)(\hat{\mu}_i\cdot\hat{E}_c)(\hat{\mu}_i\cdot\hat{E}_b)(\hat{\mu}_i\cdot\hat{E}_a)\rangle$, is the value of the orientational four-point correlation function that was evaluated in Figure 3; $|\mu_i|^4$ is the magnitude of the dipole to the fourth power; t_3 and t_1 are the coherence times in the probe and pump dimensions, respectively; T_2 is the dephasing time (set to 2 ps for these simulations). To create the total rephasing spectra and total nonrephasing spectra, the third-order response function for each Feynman pathway that contributes to the diagonal peaks, the cross-peaks, and the excited state absorptions are summed together. Each of these third-order response functions is provided in the Supporting Information (eq S20−S25). A Fourier transform along both the pump and probe dimension is performed, taking the spectra to the frequency domain. The nonrephasing and rephasing spectra in the frequency domain are then added together to obtain a purely absorptive spectrum. The spectrum produced represents changes that are purely due to the orientation of the system under investigation. Table S1 and Table S2 contain the specific parameters for each simulated 2D spectra.

For the surface response, we choose to investigate the signal produced when $\theta = 30°$ and $\psi = 30°$ (other conditions have also been calculated, see Figure S4). The bulk two-dimensional spectra are also simulated. We also choose to investigate the complementary polarization conditions, YYYY and YYYX, as well. While these polarization conditions are the same for the bulk case (as you are effectively just rotating the plane by 90°), for the surface system, the order in which the interactions between X and Y occur matter, similar to the difference to left vs

https://dx.doi.org/10.1021/acs.jpca.9b11791
J. Phys. Chem. A 2020, 124, 3471−3483

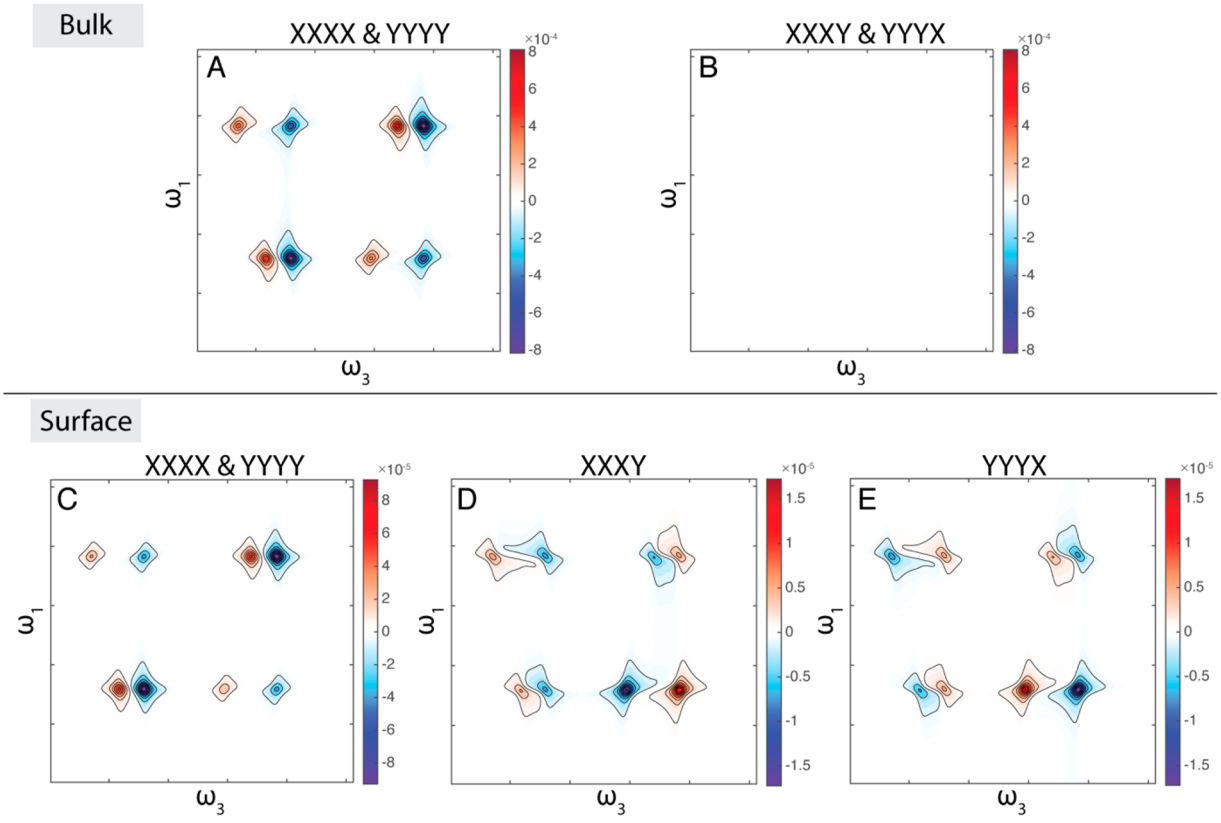

Figure 5. Simulated two-dimensional spectra for two coupled oscillators in both bulk and surface systems under four polarization conditions: XXXX, YYYY, XXXY, and YYYX. The angle between the two oscillators is $\theta_{ab} = 30°$. For the surface system, oscillator a is along the z axis, while b is in the XZ plane, as shown in Figure 1. For the surface two-dimensional spectra, $\theta = 30°$and $\psi = 30°$.

right-handed polarized light in VCD. This leads to different responses in the 2D spectra as discussed below. The plotting convention we choose to use is a negative ground state bleach for the bulk isotropic system under a parallel polarization scheme. Thus, any differences from this convention are of consequence.

In Figure 5, A and B are for bulk systems. For the XXXX and YYYY cases, each pathway has the same response (Figure S6), resulting in the same 2D spectrum. The probe frequency is plotted on the horizontal axis, while the pump frequency is plotted on the vertical axis. The spectrum is unnormalized, and the resulting intensity is purely due to the orientation of the dipoles and the transition dipole strength. We see two diagonal peaks, one for each oscillator, with both a negative ground state bleach (blue) and a positive excited state absorption (red). Both an upper ($j-i$) and lower ($i-j$) cross-peak are seen. For the bulk system investigated with the XXXY and YYYX, once again the pathway responses are the same (Figure S6), leading to the same 2D spectrum. However, the value of the pathways in a XXXY or YYYX polarization configuration is zero, leading to zero signal in the 2D spectrum, as seen by the colormap of the spectra in Figure 5B.

The 2D spectra of the surface are different in intensity and sign from that of the bulk and are shown in Figure 5C−E. Again, the XXXX and YYYY responses are the same for the surface system (Figure S7), and thus produce the same spectrum (Figure 5C). Two diagonal peaks with a ground state bleach and excited state absorption are observed, as well as upper and lower cross-peaks. In the XXXY polarization configuration of the surface (Figure 5D), the 2D spectrum is quite different than the all parallel polarization case. Our conventional diagonal peaks associated with the *iiii* and *jjjj* pathways are completely gone, consistent with the values of the pathways seen in Figure 3. Instead, all we observe are cross-peaks. The nonrephasing on-diagonal cross-peak from the *ijji* and *jiij* pathway appear in place of the purely absorptive diagonal peaks. The two on-diagonal cross-peaks are opposite in sign as predicted in Figure 4D,E. The nonrephasing *ijji* pathway leads to a negative ground state bleach for the lower on-diagonal cross-peak, while the nonrephasing *jiij* pathways lead to a positive ground state bleach for the upper on-diagonal cross-peak. Two off-diagonal cross-peaks are present in the XXXY spectrum in both the upper and lower quadrant, just like in the XXXX/YYYY polarization. However, in the XXXY case, the upper and lower cross-peak are opposite in sign and different in magnitude. The lower cross-peak has a flipped sign as compared to the off-diagonal cross-peak in the XXXX/YYYY case. Here, the ground state bleach of the lower off-diagonal cross-peak is now positive (red) while the excited state absorption is negative (blue) (Figure 5D). The upper cross-peak, however, maintains the conventional sign of the ground state bleach and excited state absorption. Although the magnitude is less than that of the lower off-diagonal cross-peak. This can be explained by considering the contributions of the *jjii* and *jiji* pathways to that cross-peak. The pathways that contribute to the $j-i$ off-diagonal cross-peak are the rephasing *jiji*, rephasing *jjii*, and nonrephasing *jjii* pathways. As seen in Figure 3, the *jjii* pathway is positive while the *jiji* pathway is negative. Thus, the *jiji* pathways cancel with one of the *jjii* pathways, leaving only one contribution from the *jjii* pathway. This causes the upper diagonal cross-peak to be $^1/_3$ the signal strength of the lower diagonal cross-peak.

https://dx.doi.org/10.1021/acs.jpca.9b11791
J. Phys. Chem. A 2020, 124, 3471−3483

Furthermore, the surface spectrum is also different in the YYYX case (Figure 5E). Here, the spectrum is just the negative of the XXXY case, as predicted by Table 1. This makes intuitive sense when the order of the pulses is considered. In the XXXY configuration, the first three interactions are in the X direction and the last is in the Y direction. This rotation of light is in the clockwise direction (relative to the axes defined in Figure 1A). When the YYYX polarization configuration is used, this is equivalent to rotating light in a counterclockwise direction. Moreover, if the −Y−Y−YX polarization condition is used, the sign of the signals follows that of the XXXY configuration as the interactions are still performed in a clockwise matter. The −X−X−XY polarization, follows that of the YYYX configuration by the same argument. The pathway responses for the YYYX polarization are plotted in Figure S7.

To further understand the origin of the flipped sign of the off-diagonal cross-peaks, we consider how the lower cross-peak depends on θ_{ab}. Figure S3 shows the 2D spectra in the XXXX and XXXY configurations for the same two oscillators depicted in Figure 1, but with different values of θ_{ab}. The lower off-diagonal cross-peak does not always flip sign for the XXXY configuration when compared to the XXXX case. The origin of this difference comes in the sign of the response for the *iijj* and *ijij* pathways. Figure 6 plots these pathway responses for a value of $\theta = 30°$ and $\psi = 30°$ as a function of θ_{ab}. In both the XXXY and YYYX polarization configuration, *iijj* and *ijij* are equivalent and shown in blue, whereas *ijji* is plotted in red. In the XXXY case, the *iijj* and *ijij* path is negative for θ_{ab} less than 49.11°, and positive for θ_{ab} greater than 49.11° (Figure 6A). Conversely, in the YYYX case, when θ_{ab} is less than 49.11°, the *iijj* and *ijij* responses are positive and become negative when θ_{ab} is greater than 49.11° (Figure 6B). The *ijji* pathway follows the opposite trend of the *iijj* and *ijij* pathways in both the XXXY and YYYX cases. From the simulated 2D spectra in Figure 5 and Figure S3, it is clear that the off-diagonal cross-peaks have the opposite sign, relative to the all parallel detection case, when these *iijj* and *ijij* pathways have a negative value. This flipping dependence of the cross-peaks as a function of θ_{ab} provides insight into the orientation of the molecule at the surface. By measuring both XXXY and YYYX, we can obtain insight into the value of θ_{ab} depending on in which spectrum the cross-peak has a flipped sign relative to the parallel case. If the cross-peak sign has flipped in the XXXY case, then θ_{ab} is less than 49.11°, while if it is flipped in the YYYX case, then θ_{ab} is greater than 49.11°. However, it should be noted that the θ_{ab} at which the flipped sign of the cross-peak occurs also depends on the θ and ψ values of the surface system (Figure S8), as well as on the dipole's original orientation relative to the surface (Figure S9). The same analysis can also be done with the upper cross-peak.

In the proposed singularly cross-polarized scheme, enhancement techniques can be used as long as the polarization is retained. All types of experimental geometry may be used as well (i.e., BOXCARS, pump−probe, or ATR). While the calculations presented in the main text assume an incident angle of all three pulses to be normal to the surface (i.e., collinear), this is unrealistic in experimental practice. Figure S10 shows how the pathway responses (*iiii, jjjj, ijij, iijj, ijji, jiji, jjii, jiji*) and the diagonal and cross-peak signals change as a function of incident angle between the pump and probe for different surface orientations. Overall, the trends discussed above are independent of the incident angle on the sample. The diagonal peak pathways are zero when using a singularly cross-polarized scheme, and the sign of the cross-peak changes. However, the intensity of the signal does decrease as the incident angle between the pump and probe increases. When considering the intensity of the signal to quantify the orientation and structure of a system, the polarization relative to the surface must also be considered.

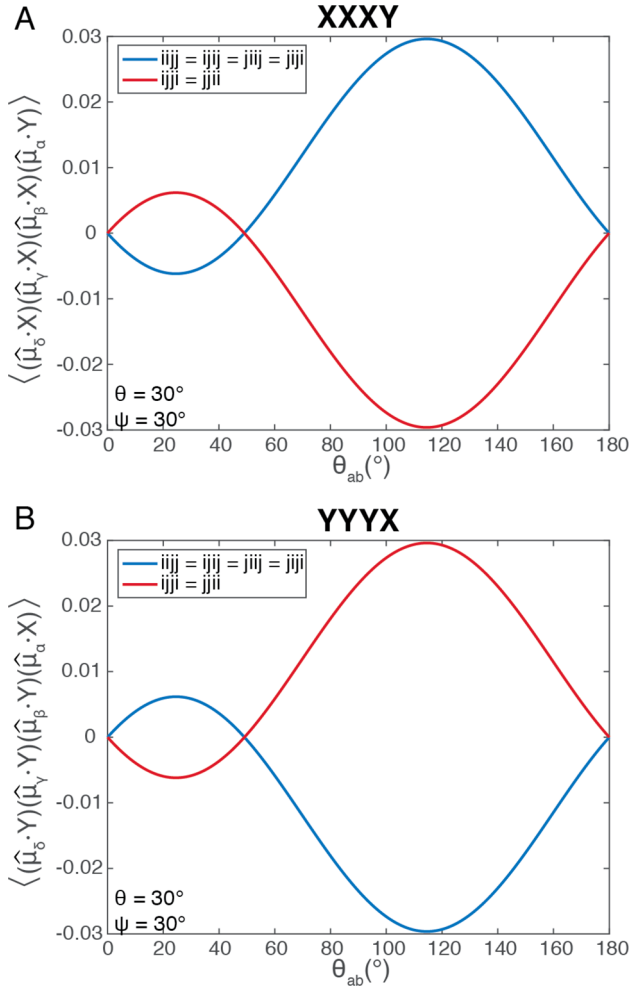

Figure 6. Cross-peak pathway dependence on θ_{ab} for $\theta = 30°$ and for $\psi = 30°$ for XXXY and YYYX polarization conditions. *iijj, ijij, jiij,* and *jiji* pathways are equivalent for the XXXY and YYYX functions and are plotted in blue. The *ijji* and *jjii* pathways is plotted in red.

Comparison to SFG Spectroscopy and VCD. The singularly cross-polarized technique above builds off of previous work by Simpson and Mukamel and demonstrates that *surface-specific* information can be obtained with a third-order spectroscopy.[42−45] In this section, we compare the proposed technique to VCD, SFG spectroscopy, chirality-induced 2D IR, and conventional 2D spectroscopy to provide insight into the similarities and differences between these spectroscopies. Table 2 provides a summary of these comparisons.

The first comparison made in Table 2 across the five spectroscopies of interest is the order of the susceptibility measured. VCD is a linear spectroscopy, while the three 2D spectroscopies (chiral induced, conventional, singularly cross-polarized) are nonlinear third-order experiments. SFG spectroscopy is a nonlinear even-order technique that measures the second-order susceptibility. These differences influence what determines the intensity of the signal and the type of systems that can be studied.

https://dx.doi.org/10.1021/acs.jpca.9b11791
J. Phys. Chem. A 2020, 124, 3471−3483

Table 2. Comparison of Different Spectroscopies to Singularly Cross-Polarized 2D Spectroscopy

category	VCD	SFG	chiral induced 2D IR	conventional 2D optical spectroscopy	singularly cross-polarized 2D spectroscopy	
susceptibility order	χ^1	χ^2	χ^3	χ^3	χ^3	χ^3
signal intensity	$\propto\mu$m	$\propto\alpha\mu$	$\propto r\mu^4$	$\propto\mu^4$	$\propto\mu_i^2\mu_j^2$	$\propto\mu_i^2\mu_j^2$
systems studied	bulk	interfaces surfaces	bulk	bulk	interfaces surfaces	bulk
molecule requirements	chiral	chiral or achiral	chiral	chiral or achiral	chiral or achiral	chiral

SFG spectroscopy is the only even-ordered spectroscopy considered in the table (although further comparisons could be made to 2D SFG spectroscopy). The signal intensity of SFG spectroscopy relies on both the transition dipole (μ) and the Raman tensor (or transition polarizability) (α) of the vibration of interest. SFG spectroscopy also measures interfaces and surfaces with *surface-specificity*, as the SFG signal of bulk centrosymmetric systems go to zero. This is similar to singularly cross-polarized 2D spectroscopy that also measures signals from interfaces and surfaces. However, the important distinction is that for the third-order case the signal relies on the transition dipole squared of two coupled states ($\mu_i^2\mu_j^2$). Thus, for the singularly cross-polarized 2D spectroscopy, the molecules at the surface must be coupled in a nonparallel way to produce cross-peaks in the 2D spectra of the surface. In conventional 2D spectroscopy, the signal strength of a single state is dependent on the transition dipole to the fourth. These types of signals are not observed in the singularly cross-polarized technique. But the cross-peak signal intensity observed in conventional 2D spectra is equivalent to what is observed in the singularly cross-polarized scheme, meaning that they depend on the transition dipole squared of two coupled states. Conventional 2D spectroscopy has been used to study bulk systems extensively,[58,59] although, there are examples of 2D spectroscopy studying monolayers and surfaces in a *surface-sensitive* way.[19] The singularly cross-polarized technique would complement existing even-ordered spectroscopies, such as SFG spectroscopy, by providing structural sensitivity due to coupling, dynamics through line shape analysis, and other observables typical of 2D IR/vis spectroscopies, but for surfaces specifically.

VCD and chirality induced 2D IR both rely on measuring bulk chiral molecules. The signal strength of VCD is determined by the rotational strength (r), or the dot product of the transition dipole and the magnetic dipole (μm), which can be rewritten as the cross-product of two transition dipoles.[60] Chirality induced 2D IR is the two-dimensional equivalent of VCD, the signal strength of which depends on the rotational strength and the transition dipole to the fourth power ($r\mu^4$).[42,43] The chiral induced signals are detected by using the same pulse sequence as proposed for the singularly cross-polarized 2D spectroscopy: XXXY. The difference between chirality induced 2D IR and singularly cross-polarized 2D spectroscopy is the type of systems and molecules measured. In the chirality induced 2D spectroscopy, bulk chiral molecules are measured, resulting in both diagonal peak and cross-peaks associated with 2D spectroscopy in general. For the singularly cross-polarized technique proposed here, the XXXY pulse sequence is applied to a surface system, removing the requirement that the molecule be chiral. Moreover, the singularly cross-polarized technique is completely dipole allowed. However, only cross-peaks are observed in this spectrum as described above. VCD, chirality induced 2D IR, and singularly cross-polarized 2D spectroscopy all measure reduced symmetry systems, but how the symmetry is reduced is in different ways. For VCD and chirality induced 2D IR, the molecules themselves are chiral, and thus have reduced symmetry, while for the technique proposed here, the surface induces a reduced symmetry system. Thus, all three of the spectroscopies can be considered "chiral" methods. Chiral methods work for chiral molecules in the bulk as well as chiral and achiral molecules on a surface. Thus, the singularly cross-polarized technique is applicable to bulk chiral molecules, as well as chiral and achiral molecules on a surface. In the case for which an interface of where the molecules probed are chiral, the technique proposed here is no longer *surface-specific* if there is bulk solution present the sample. Here, the signals from both the chiral bulk molecules and the chiral surface molecules will be detected in the singularly cross-polarized method (Table 2). This also true when SFG spectroscopy is applied to chiral bulk molecules and the visible beam is resonant with the electronic state of the chiral molecule.[61−63] However, these bulk chiral SFG signals are different from the surface chiral SFG signals probed with a chiral SFG method that is indeed *surface-specific*.[64−68]

CONCLUSIONS

We have computed how to extend third-order spectroscopies, such as 2D infrared and 2D electronic spectroscopies, into the *surface-specific* regime. We do this by taking advantage of how the macroscopic orientation of molecules at the surface is mapped onto the third-order signal under specific polarizations. By using a singularly cross-polarized detection scheme, all peaks in the bulk system, as well as diagonal peaks in the surface system, are zero. This leaves only cross-peaks from the ordered surface in the detected spectrum. Previously, only even-ordered spectroscopies, such as SFG spectroscopy, have been able to discern between signals from the bulk and the surface, by only measuring the response from the molecules at the surface or interface. Our proposed polarization scheme provides third-order spectroscopies that same capability typically only associated with even-ordered spectroscopies. Moreover, the dependence of the sign of the cross-peaks with the polarization used provides evidence of signals only from the surface and not from the bulk. The proposed method is a completely dipole allowed chiral method, as the sign of the signal depends of the macroscopic polarization of light. This same pulse sequence has been demonstrated to work for bulk chiral molecules.[42,43] We propose to use the XXXY polarization condition on a surface, which induces chirality to the system independent of whether the molecules on the surface are chiral or not.

Previously, different polarization conditions have been used to specifically interrogate cross-peaks in bulk systems.[51,69−71] Here, we provide an approach to probe cross-peaks from surface systems without influence from the bulk. These surface systems must be biaxial, meaning that there is long-range order over two axis. In our simulations, the surface system we studied had defined tilt (θ) and twist (ψ) angles. In practice, this technique might be used to study any ordered biaxial system, such as a monolayer, crystal, or exposed and buried interfaces. These

https://dx.doi.org/10.1021/acs.jpca.9b11791
J. Phys. Chem. A 2020, 124, 3471−3483

systems would include both chemisorbed and physiosorbed self-assembled monolayers, ordered two-dimensional thin films, and membrane proteins in lipid bilayers. Despite a low number of molecules in these systems (1 nmol/cm^2 or less),[72] 2D spectroscopies are capable of such measurements.[16,19,22,24,28,73,74]

The singularly cross-polarized 2D spectroscopy proposed here does not hold for every system. The molecule or molecules of interest must have transition dipoles that are coupled in a nonparallel way to create cross-peaks. For vibrational spectroscopy, this is common for small molecules with multiple functional groups. For electronic spectroscopy, coupled chromophores or different electronic states in the same molecule are applicable. However, cross-peaks from vibrational progressions in the ground or excited state would not work as the transition dipoles of those transitions are usually parallel. The system can have a variation in the twist and tilt angle of the transitions with respect to the surface; however, the size of the variation will impact the size of the observed signals in the singularly cross-polarized scheme. The size of the observed signal will also be modulated by how well the polarization of light is maintained, with imperfect polarization leading to decreased signal.

In this work, the singularly cross-polarized scheme proposed broadens the capabilities of an already impressive technique. From observing coherences in light harvesting proteins,[75−77] to probing the singlet fission process of TIPS-pentacene,[78] to monitoring the chemical exchange of hydrogen-bond formation,[79,80] and detecting changes in protein structure and aggregation,[58,81,82] 2D spectral measurements of bulk systems provide insight on both the structure and dynamics of such systems.[83] These same types of measurements can now be done at a surface, of which the structure and dynamics may be altered due to surface packing, surface diffusion, and differences in solvation.

■ ASSOCIATED CONTENT

Supporting Information

The Supporting Information is available free of charge at https://pubs.acs.org/doi/10.1021/acs.jpca.9b11791.

Additional information on the angle dependence (θ, ψ, θ_{ab}) and orientational dependence of the signal, evaluated four-point correlation functions, and inputs for the simulated 2D spectra (PDF)

■ AUTHOR INFORMATION

Corresponding Author

Martin T. Zanni − *Department of Chemistry, University of Wisconsin-Madison, Madison, Wisconsin 53706, United States;* orcid.org/0000-0001-7191-9768; Phone: 608-262-4783; Email: zanni@chem.wisc.edu

Authors

Megan K. Petti − *Department of Chemistry, University of Wisconsin-Madison, Madison, Wisconsin 53706, United States;* orcid.org/0000-0001-7381-9701

Joshua S. Ostrander − *Department of Chemistry, University of Wisconsin-Madison, Madison, Wisconsin 53706, United States;* orcid.org/0000-0002-6338-6639

Erin R. Birdsall − *Department of Chemistry, University of Wisconsin-Madison, Madison, Wisconsin 53706, United States*

Miriam Bohlmann Kunz − *Department of Chemistry, University of Wisconsin-Madison, Madison, Wisconsin 53706, United States;* orcid.org/0000-0002-7852-159X

Zachary T. Armstrong − *Department of Chemistry, University of Wisconsin-Madison, Madison, Wisconsin 53706, United States;* orcid.org/0000-0002-1207-6171

Ariel M. Alperstein − *Department of Chemistry, University of Wisconsin-Madison, Madison, Wisconsin 53706, United States;* orcid.org/0000-0003-1310-1081

Complete contact information is available at: https://pubs.acs.org/10.1021/acs.jpca.9b11791

Notes

The authors declare the following competing financial interest(s): Martin Zanni is a co-owner of PhaseTech Spectroscopy, Inc., which manufactures ultrafast pulse shapers and 2D spectrometers.

■ ACKNOWLEDGMENTS

This research was funded by NSF CHE 1665110, NIH R21AG061602, and NIH R01DK79895. M.T.Z. was supported by NIH R21AG061602 and R01DK079895. E.R.B. is supported by the NIGMS T32GM008349.

■ REFERENCES

(1) Page, R. C.; Kim, S.; Cross, T. A. Transmembrane Helix Uniformity Examined by Spectral Mapping of Torsion Angles. *Structure* **2008**, *16*, 787−797.

(2) Özdirekcan, S.; Rijkers, D. T. S.; Liskamp, R. M. J.; Killian, J. A. Influence of Flanking Residues on Tilt and Rotation Angles of Transmembrane Peptides in Lipid Bilayers. A Solid-State 2H NMR Study. *Biochemistry* **2005**, *44*, 1004−1012.

(3) Ho, J.; Psciuk, B. T.; Chase, H. M.; Rudshteyn, B.; Upshur, M. A.; Fu, L.; Thomson, R. J.; Wang, H. F.; Geiger, F. M.; Batista, V. S. Sum Frequency Generation Spectroscopy and Molecular Dynamics Simulations Reveal a Rotationally Fluid Adsorption State of α-Pinene on Silica. *J. Phys. Chem. C* **2016**, *120*, 12578−12589.

(4) Nihonyanagi, S.; Yamaguchi, S.; Tahara, T. Ultrafast Dynamics at Water Interfaces Studied by Vibrational Sum Frequency Generation Spectroscopy. *Chem. Rev.* **2017**, *117*, 10665−10693.

(5) Zhang, Z.; Piatkowski, L.; Bakker, H. J.; Bonn, M. Ultrafast Vibrational Energy Transfer at the Water/Air Interface Revealed by Two-Dimensional Surface Vibrational Spectroscopy. *Nat. Chem.* **2011**, *3*, 888−893.

(6) Yang, P.; Glukhova, A.; Tesmer, J. J. G.; Chen, Z. Membrane Orientation and Binding Determinants of G Protein-Coupled Receptor Kinase 5 as Assessed by Combined Vibrational Spectroscopic Studies. *PLoS One* **2013**, *8*, 1−11.

(7) Xiao, D.; Fu, L.; Liu, J.; Batista, V. S.; Yan, E. C. Y. Amphiphilic Adsorption of Human Islet Amyloid Polypeptide Aggregates to Lipid/Aqueous Interfaces. *J. Mol. Biol.* **2012**, *421*, 537−547.

(8) Yan, C.; Yuan, R.; Nishida, J.; Fayer, M. D. Structural Influences on the Fast Dynamics of Alkylsiloxane Monolayers on SiO2 Surfaces Measured with 2D IR Spectroscopy. *J. Phys. Chem. C* **2015**, *119*, 16811−16823.

(9) Yan, C.; Yuan, R.; Pfalzgraff, W. C.; Nishida, J.; Wang, L.; Markland, T. E.; Fayer, M. D. Unraveling the Dynamics and Structure of Functionalized Self-Assembled Monolayers on Gold Using 2D IR Spectroscopy and MD Simulations. *Proc. Natl. Acad. Sci. U. S. A.* **2016**, *113*, 4929−4934.

(10) Ding, B.; Laaser, J. E.; Liu, Y.; Wang, P.; Zanni, M. T.; Chen, Z. Site-Specific Orientation of an a-Helical Peptide Ovispirin-1 from Isotope-Labeled SFG Spectroscopy. *J. Phys. Chem. B* **2013**, *117*, 14625−14634.

(11) Stein, R. S. The X-Ray Diffraction, Birefringence, and Infrared Dichroism of Stretched Polyethylene. III. Biaxial Orientation. *J. Polym. Sci.* **1958**, *31*, 335−343.
(12) Uejo, H.; Hoshino, S. Structure of Biaxially Oriented Polypropylene Film. *J. Appl. Polym. Sci.* **1970**, *14*, 317−328.
(13) Rhee, S.; White, J. L. Crystal Structure and Morphology of Biaxially Oriented Polyamide 12 Films. *J. Polym. Sci., Part B: Polym. Phys.* **2002**, *40*, 1189−1200.
(14) Krishnaswamy, R. K. A Method to Characterize the Biaxial Orientation of The. *J. Polym. Sci., Part B: Polym. Phys.* **2000**, *38*, 182−193.
(15) Rosenfeld, D. E.; Nishida, J.; Yan, C.; Gengeliczki, Z.; Smith, B. J.; Fayer, M. D. Dynamics of Functionalized Surface Molecular Monolayers Studied with Ultrafast Infrared Vibrational Spectroscopy. *J. Phys. Chem. C* **2012**, *116*, 23428−23440.
(16) Rosenfeld, D. E.; Gengeliczki, Z.; Smith, B. J.; Stack, T. D. P.; Fayer, M. D. Structural Dynamics of a Catalytic Monolayer Probed by Ultrafast 2D IR Vibrational Echoes. *Science* **2011**, *334*, 634−639.
(17) Leube, H. F.; Finkelmann, H. Optical Investigations on a Liquid-crystalline Side-chain Polymer with Biaxial Nematic and Biaxial Smectic A Phase. *Makromol. Chem.* **1991**, *192*, 1317−1328.
(18) Yuan, W. Z.; Yu, Z. Q.; Lu, P.; Deng, C.; Lam, J. W. Y.; Wang, Z.; Chen, E. Q.; Ma, Y.; Tang, B. Z. High Efficiency Luminescent Liquid Crystal: Aggregation-Induced Emission Strategy and Biaxially Oriented Mesomorphic Structure. *J. Mater. Chem.* **2012**, *22*, 3323−3326.
(19) Kraack, J. P.; Hamm, P. Surface-Sensitive and Surface-Specific Ultrafast Two-Dimensional Vibrational Spectroscopy. *Chem. Rev.* **2017**, *117*, 10623−10664.
(20) Ghosh, A.; Ho, J.-J.; Serrano, A. L.; Skoff, D. R.; Zhang, T.; Zanni, M. T. Two-Dimensional Sum-Frequency Generation (2D SFG) Spectroscopy: Summary of Principles and Its Application to Amyloid Fiber Monolayers. *Faraday Discuss.* **2015**, *177*, 493−505.
(21) Kraack, J. P.; Kaech, A.; Hamm, P. Surface Enhancement in Ultrafast 2D ATR IR Spectroscopy at the Metal-Liquid Interface. *J. Phys. Chem. C* **2016**, *120*, 3350−3359.
(22) Lotti, D.; Hamm, P.; Kraack, J. P. Surface-Sensitive Spectro-Electrochemistry Using Ultrafast 2D ATR IR Spectroscopy. *J. Phys. Chem. C* **2016**, *120*, 2883−2892.
(23) Kraack, J. P.; Frei, A.; Alberto, R.; Hamm, P. Ultrafast Vibrational Energy Transfer in Catalytic Monolayers at Solid-Liquid Interfaces. *J. Phys. Chem. Lett.* **2017**, *8*, 2489−2495.
(24) Nishida, J.; Yan, C.; Fayer, M. D. Enhanced Nonlinear Spectroscopy for Monolayers and Thin Films in Near-Brewster's Angle Reflection Pump-Probe Geometry. *J. Chem. Phys.* **2017**, *146*, 094201.
(25) Xiong, W.; Zanni, M. T. Signal Enhancement and Background Cancellation in Collinear Two-Dimensional Spectroscopies. *Opt. Lett.* **2008**, *33*, 1371.
(26) Lotti, D.; Hamm, P.; Kraack, J. P. Surface-Sensitive Spectro-Electrochemistry Using Ultrafast 2D ATR IR Spectroscopy. *J. Phys. Chem. C* **2016**, *120*, 2883−2892.
(27) Kraack, J. P.; Lotti, D.; Hamm, P. 2D Attenuated Total Reflectance Infrared Spectroscopy Reveals Ultrafast Vibrational Dynamics of Organic Monolayers at Metal-Liquid Interfaces. *J. Chem. Phys.* **2015**, *142*, 212413.
(28) Kraack, J. P.; Kaech, A.; Hamm, P. Surface Enhancement in Ultrafast 2D ATR IR Spectroscopy at the Metal-Liquid Interface. *J. Phys. Chem. C* **2016**, *120*, 3350−3359.
(29) Kraack, J. P.; Hamm, P. Vibrational Ladder-Climbing in Surface-Enhanced, Ultrafast Infrared Spectroscopy. *Phys. Chem. Chem. Phys.* **2016**, *18*, 16088−16093.
(30) Rey, N. G.; Dlott, D. D. Studies of Electrochemical Interfaces by Broadband Sum Frequency Generation. *J. Electroanal. Chem.* **2017**, *800*, 114−125.
(31) Wang, Z.; Carter, J. A.; Lagutchev, A.; Yee, K. K.; Seong, N. H.; Cahilll, D. G.; Dlott, D. D. Ultrafast Flash Thermal Conductance of Molecular Chains. *Science* **2007**, *317*, 787−790.
(32) Bredenbeck, J.; Ghosh, A.; Smits, M.; Bonn, M. Ultrafast Two Dimensional-Infrared Spectroscopy of a Molecular Monolayer. *J. Am. Chem. Soc.* **2008**, *130*, 2152−2153.
(33) Ghosh, A.; Smits, M.; Bredenbeck, J.; Dijkhuizen, N.; Bonn, M. Femtosecond Time-Resolved and Two-Dimensional Vibrational Sum Frequency Spectroscopic Instrumentation to Study Structural Dynamics at Interfaces. *Rev. Sci. Instrum.* **2008**, *79*, 093907.
(34) Bredenbeck, J.; Ghosh, A.; Nienhuys, H.-K.; Bonn, M. Interface-Specific Ultrafast Two-Dimensional Vibrational Spectroscopy. *Acc. Chem. Res.* **2009**, *42*, 1332−1342.
(35) Zhu, X. D.; Suhr, H.; Shen, Y. R. Surface Vibrational Spectroscopy by Infrared-Visible Sum Frequency Generation. *Phys. Rev. B: Condens. Matter Mater. Phys.* **1987**, *35*, 3047−3050.
(36) Shen, Y. R. Surface Properties Probed by Second-Harmonic and Sum-Frequency Generation. *Nature* **1989**, *337*, 519−525.
(37) Lambert, A. G.; Davies, P. B.; Neivandt, D. J. Implementing the Theory of Sum Frequency Generation Vibrational Spectroscopy: A Tutorial Review. *Appl. Spectrosc. Rev.* **2005**, *40*, 103−145.
(38) Geiger, F. M. Second Harmonic Generation, Sum Frequency Generation, and $\chi^{(3)}$: Dissecting Environmental Interfaces with a Nonlinear Optical Swiss Army Knife. *Annu. Rev. Phys. Chem.* **2009**, *60*, 61−83.
(39) Rhee, H.; Kim, S. S.; Jeon, S. J.; Cho, M. Femtosecond Measurements of Vibrational Circular Dichroism and Optical Rotatory Dispersion Spectra. *ChemPhysChem* **2009**, *10*, 2209−2211.
(40) Rhee, H.; June, Y. G.; Lee, J. S.; Lee, K. K.; Ha, J. H.; Kim, Z. H.; Jeon, S. J.; Cho, M. Femtosecond Characterization of Vibrational Optical Activity of Chiral Molecules. *Nature* **2009**, *458*, 310−313.
(41) Kwac, K.; Lee, K. K.; Han, J. B.; Oh, K. I.; Cho, M. Classical and Quantum Mechanical/Molecular Mechanical Molecular Dynamics Simulations of Alanine Dipeptide in Water: Comparisons with IR and Vibrational Circular Dichroism Spectra. *J. Chem. Phys.* **2008**, *128*, 105106.
(42) Zhuang, W.; Sgourakis, N. G.; Li, Z.; Garcia, A. E.; Mukamel, S. Discriminating Early Stage A 42 Monomer Structures Using Chirality-Induced 2DIR Spectroscopy in a Simulation Study. *Proc. Natl. Acad. Sci. U. S. A.* **2010**, *107*, 15687−15692.
(43) Abramavicius, D.; Zhuang, W.; Mukamel, S. Probing Molecular Chirality via Excitonic Nonlinear Response. *J. Phys. B: At., Mol. Opt. Phys.* **2006**, *39*, 5051−5066.
(44) Davis, R. P.; Moad, A. J.; Goeken, G. S.; Wampler, R. D.; Simpson, G. J. Selection Rules and Symmetry Relations for Four-Wave Mixing Measurements of Uniaxial Assemblies. *J. Phys. Chem. B* **2008**, *112*, 5834−5848.
(45) Deng, F.; Ulcickas, J. R. W.; Simpson, G. J. Theoretical Foundation for Electric-Dipole-Allowed Chiral-Specific Fluorescence Optical Rotary Dispersion (F-ORD) from Interfacial Assemblies. *J. Phys. Chem. Lett.* **2016**, *7*, 4248−4252.
(46) Mukamel, S. *Principles of Nonlinear Optical Spectroscopy*; Oxford University Press: New York, 1995.
(47) Cho, M. *Two-Dimensional Optical Spectroscopy*; Taylor & Francis Group: Boca Raton, 2009.
(48) Hamm, P.; Zanni, M. T. *Concepts and Methods of 2D Infrared Spectroscopy*; Cambridge University Press: New York, 2011.
(49) Khalil, M.; Demirdöven, N.; Tokmakoff, A. Coherent 2D IR Spectroscopy: Molecular Structure and Dynamics in Solution. *J. Phys. Chem. A* **2003**, *107*, 5258−5279.
(50) Hochstrasser, R. M. Two-Dimensional Spectroscopy at Infrared and Optical Frequencies. *Proc. Natl. Acad. Sci. U. S. A.* **2007**, *104*, 14190−14196.
(51) Read, E. L.; Engel, G. S.; Calhoun, T. R.; Mančal, T.; Tae, K. A.; Blankenship, R. E.; Fleming, G. R. Cross-Peak-Specific Two-Dimensional Electronic Spectroscopy. *Proc. Natl. Acad. Sci. U. S. A.* **2007**, *104*, 14203−14208.
(52) Pisliakov, A. V.; Mančal, T.; Fleming, G. R. Two-Dimensional Optical Three-Pulse Photon Echo Spectroscopy. II. Signatures of Coherent Electronic Motion and Exciton Population Transfer in Dimer Two-Dimensional Spectra. *J. Chem. Phys.* **2006**, *124*, 234505.

https://dx.doi.org/10.1021/acs.jpca.9b11791
J. Phys. Chem. A 2020, 124, 3471−3483

(53) Hochstrasser, R. M. Two-Dimensional IR-Spectroscopy: Polarization Anisotropy Effects. *Chem. Phys.* **2001**, *266*, 273−284.
(54) Laaser, J. E.; Zanni, M. T. Extracting Structural Information from the Polarization Dependence of One- and Two-Dimensional Sum Frequency Generation Spectra. *J. Phys. Chem. A* **2013**, *117*, 5875−5890.
(55) Nishida, J.; Fayer, M. D. Theory of Third-Order Spectroscopic Methods to Extract Detailed Molecular Orientational Dynamics for Planar Surfaces and Other Uniaxial Systems. *J. Chem. Phys.* **2014**, *140*, 144702.
(56) Ataka, K.; Giess, F.; Knoll, W.; Naumann, R.; Haber-Pohlmeier, S.; Richter, B.; Heberle, J. Oriented Attachment and Membrane Reconstitution of His-Tagged Cytochrome c Oxidase to a Gold Electrode: In Situ Monitoring by Surface-Enhanced Infrared Absorption Spectroscopy. *J. Am. Chem. Soc.* **2004**, *126*, 16199−16206.
(57) Ataka, K.; Stripp, S. T.; Heberle, J. Surface-Enhanced Infrared Absorption Spectroscopy (SEIRAS) to Probe Monolayers of Membrane Proteins. *Biochim. Biophys. Acta, Biomembr.* **2013**, *1828*, 2283−2293.
(58) Ghosh, A.; Ostrander, J. S.; Zanni, M. T. Watching Proteins Wiggle: Mapping Structures with Two-Dimensional Infrared Spectroscopy. *Chem. Rev.* **2017**, *117*, 10726−10759.
(59) Ganim, Z.; Chung, H. S.; Smith, A. W.; DeFlores, L. P.; Jones, K. C.; Tokmakoff, A. Amide I Two-Dimensional Infrared Spectroscopy of Proteins. *Acc. Chem. Res.* **2008**, *41*, 432−441.
(60) Krummel, A. T.; Zanni, M. T. Interpreting DNA Vibrational Circular Dichroism Spectra Using a Coupling Model from Two-Dimensional Infrared Spectroscopy. *J. Phys. Chem. B* **2006**, *110*, 24720−24727.
(61) Ji, N.; Shen, Y. R. Optically Active Sum Frequency Generation from Molecules with a Chiral Center: Amino Acids as Model Systems. *J. Am. Chem. Soc.* **2004**, *126*, 15008−15009.
(62) Belkin, M. A.; Shen, Y. R. Non-Linear Optical Spectroscopy as a Novel Probe for Molecular Chirality. *Int. Rev. Phys. Chem.* **2005**, *24*, 257−299.
(63) Zheng, R. H.; Chen, D. M.; Wei, W. M.; He, T. J.; Liu, F. C. Theoretical Investigation of Doubly Resonant IR-UV Sum-Frequency Vibrational Spectroscopy of Binaphthol Chiral Solution. *J. Phys. Chem. B* **2006**, *110*, 4480−4486.
(64) Haupert, L. M.; Simpson, G. J. Chirality in Nonlinear Optics. *Annu. Rev. Phys. Chem.* **2009**, *60*, 345−365.
(65) Moad, A. J.; Simpson, G. J. A Unified Treatment of Selection Rules and Symmetry Relations for Sum-Frequency and Second Harmonic Spectroscopies. *J. Phys. Chem. B* **2004**, *108*, 3548−3562.
(66) Perry, J. M.; Moad, A. J.; Begue, N. J.; Wampler, R. D.; Simpson, G. J. Electronic and Vibrational Second-Order Nonlinear Optical Properties of Protein Secondary Structural Motifs. *J. Phys. Chem. B* **2005**, *109*, 20009−20026.
(67) Simpson, G. J. Molecular Origins of the Remarkable Chiral Sensitivity of Second-Order Nonlinear Optic. *ChemPhysChem* **2004**, *5*, 1301−1310.
(68) Fu, L.; Liu, J.; Yan, E. C. Y. Chiral Sum Frequency Generation Spectroscopy for Characterizing Protein Secondary Structures at Interfaces. *J. Am. Chem. Soc.* **2011**, *133*, 8094−8097.
(69) Mehlenbacher, R. D.; McDonough, T. J.; Kearns, N. M.; Shea, M. J.; Joo, Y.; Gopalan, P.; Arnold, M. S.; Zanni, M. T. Polarization-Controlled Two-Dimensional White-Light Spectroscopy of Semiconducting Carbon Nanotube Thin Films. *J. Phys. Chem. C* **2016**, *120*, 17069−17080.
(70) Zanni, M. T.; Ge, N.-H.; Kim, Y. S.; Hochstrasser, R. M. Two-Dimensional IR Spectroscopy Can Be Designed to Eliminate the Diagonal Peaks and Expose Only the Crosspeaks Needed for Structure Determination. *Proc. Natl. Acad. Sci. U. S. A.* **2001**, *98*, 11265−11270.
(71) Réhault, J.; Helbing, J. Angle Determination and Scattering Suppression in Polarization-Enhanced Two-Dimensional Infrared Spectroscopy in the Pump-Probe Geometry. *Opt. Express* **2012**, *20*, 21665.
(72) Love, J. C.; Estroff, L. A.; Kriebel, J. K.; Nuzzo, R. G.; Whitesides, G. M. Self-Assembled Monolayers of Thiolates on Metals as a Form of Nanotechnology. *Chem. Rev.* **2005**, *105*, 1103−1170.
(73) Petti, M. K.; Ostrander, J. S.; Saraswat, V.; Birdsall, E. R.; Rich, K. L.; Lomont, J. P.; Arnold, M. S.; Zanni, M. T. Enhancing the Signal Strength of Surface Sensitive 2D IR Spectroscopy. *J. Chem. Phys.* **2019**, *150*, 024707.
(74) Yan, C.; Thomaz, J. E.; Wang, Y.-L.; Nishida, J.; Yuan, R.; Breen, J. P.; Fayer, M. D. Ultrafast to Ultraslow Dynamics of a Langmuir Monolayer at the Air/Water Interface Observed with Reflection Enhanced 2D IR Spectroscopy. *J. Am. Chem. Soc.* **2017**, *139*, 16518−16527.
(75) Scholes, G. D.; Fleming, G. R.; Olaya-Castro, A.; van Grondelle, R. Lessons from Nature about Solar Light Harvesting. *Nat. Chem.* **2011**, *3*, 763−774.
(76) Scholes, G. D.; Fleming, G. R. On the Mechanism of Light Harvesting in Photosynthetic Purple Bacteria: B800 to B850 Energy Transfer. *J. Phys. Chem. B* **2000**, *104*, 1854−1868.
(77) Wang, C.; Flanagan, M. L.; McGillicuddy, R. D.; Zheng, H.; Ginzburg, A. R.; Yang, X.; Moffat, K.; Engel, G. S. Bacteriophytochrome Photoisomerization Proceeds Homogeneously Despite Heterogeneity in Ground State. *Biophys. J.* **2016**, *111*, 2125−2134.
(78) Jones, A. C.; Kearns, N. M.; Ho, J.-J.; Flach, J. T.; Zanni, M. T. Impact of Non-Equilibrium Molecular Packings on Singlet Fission in Microcrystals Observed Using 2D White-Light Microscopy. *Nat. Chem.* **2020**, *12*, 40−47.
(79) Kim, Y. S.; Hochstrasser, R. M. Chemical Exchange 2D IR of Hydrogen-Bond Making and Breaking. *Proc. Natl. Acad. Sci. U. S. A.* **2005**, *102*, 11185−11190.
(80) Fayer, M. D. Dynamics of Liquids, Molecules, and Proteins Measured with Ultrafast 2D IR Vibrational Echo Chemical Exchange Spectroscopy. *Annu. Rev. Phys. Chem.* **2009**, *60*, 21−38.
(81) Buchanan, L. E.; Dunkelberger, E. B.; Tran, H. Q.; Cheng, P.-N. N.; Chiu, C.-C. C.; Cao, P.; Raleigh, D. P.; de Pablo, J. J.; Nowick, J. S.; Zanni, M. T. Mechanism of IAPP Amyloid Fibril Formation Involves an Intermediate with a Transient Beta-Sheet. *Proc. Natl. Acad. Sci. U. S. A.* **2013**, *110*, 19285−19290.
(82) Alperstein, A. M.; Ostrander, J. S.; Zhang, T. O.; Zanni, M. T. Amyloid Found in Human Cataracts with Two-Dimensional Infrared Spectroscopy. *Proc. Natl. Acad. Sci. U. S. A.* **2019**, *116*, 6602−6607.
(83) Petti, M. K.; Lomont, J. P.; Maj, M.; Zanni, M. T. Two-Dimensional Spectroscopy Is Being Used to Address Core Scientific Questions in Biology and Materials Science. *J. Phys. Chem. B* **2018**, *122*, 1771−1780.

https://dx.doi.org/10.1021/acs.jpca.9b11791
J. Phys. Chem. A 2020, 124, 3471−3483